Chemical Papers (2024) 78:6721–6735
https://doi.org/10.1007/s11696-024-03568-2

ORIGINAL PAPER

Adsorption effectiveness and properties of an enriched activated carbon from residual biomass materials for non-polar benzene in gaseous environment

Kaan Isinkaralar[1] · Aydin Turkyilmaz[1] · Ahmad Hosseini-Bandegharaei[2,3,4] · Chander Prakash[3]

Received: 15 March 2024 / Accepted: 1 June 2024 / Published online: 23 June 2024

Abstract

During the last century, benzene (C_6H_6) has been a highly studied substance, with some acute and chronic exposures leading directly to hematologic effects detected in humans. This work reports on preparing and examining biomass-derived activated carbons (HPACs) featuring high benzene adsorptive capacity. The fundamental goal of this paper is to propose a green approach for generating HPACs from *Heracleum platytaenium* Boiss. (Cow parsnip) as woody biomass using a low-cost approach. The characterization showed that chemical activation elicits more enhanced mesoporous structure, a higher degree of graphitization, and bulk porous structure with higher specific surface area and pore volume. To minimize the use of chemicals in the manufacture of high-performance HPACs, an essential pre-pyrolysis step was implemented prior to the chemical activation of biomass by NaOH. The samples were carbonized at different temperatures (500–900 °C) and named as HPAC500, HPAC600, HPAC700, HPAC800, and HPAC900. Considering micropore volume and total surface area, HPAC600 was superior, and maximum benzene adsorption capacities were: HPAC600 (127 mg/g) > HPAC700 (117 mg/g) > HPAC800 (101 mg/g) > HPAC500 (80 mg/g) > HPAC900 (59 mg/g) at selected conditions. Freundlich, Langmuir, and pseudo-first-order (PFO) and pseudo-second-order (PSO) models were used to mathematically describe HPAC600-vapor benzene sorption on HPAC600. The kinetic findings fitted PFO with optimal values of $R^2 = 0.999$, and the isotherm model adsorption fitted Freundlich model ($R^2 = 1.000$). The finding revealed that *H. platytaenium* is a useful material for producing adsorbents, and successful testing outcomes demonstrate that *H. platytaenium* products serve as a suitable benzene absorbent.

Keywords Agricultural waste · Biomass pyrolysis · Chemical activation · Toxic chemical · Volatile organic compounds

Introduction

Potentially toxic substances remain vastly utilized in several products, which are rapidly increasing, including in-vehicle evaporative (Yue et al. 2017) and exhaust emissions (Adamović et al. 2013), gasoline and other petroleum products (Schifter et al. 2014), tobacco smoke (Fiebelkorn and Meredith 2018), synthetic rubber manufacturing industry (Perkins et al. 2019), and indoor spaces (Kozielska and Kaleta 2020; Jiang et al. 2022). Persistent volatile organic compounds (VOCs) have penetrated every aspect of our lives and become a severe threat (Arnold et al. 2013; Fang et al. 2019). Benzene (C_6H_6) is well recognized to have a depressive effect and is one of the main chemicals used as a trace pollutant in indoor air; it has become widespread in various areas (Ji et al. 2020). Uncertainties in the frequency of use, rises in the concentration amount, and the resulting increase in the amount of emissions reveal that benzene threatens

✉ Kaan Isinkaralar
kisinkaralar@kastamonu.edu.tr

Aydin Turkyilmaz
aturkyilmaz@kastamonu.edu.tr

[1] Department of Environmental Engineering, Faculty of Engineering and Architecture, Kastamonu University, 37150 Kastamonu, Türkiye

[2] Department of Chemistry, Semnan University, Semnan, Iran

[3] University Centre for Research & Development, Chandigarh University, Mohali, Punjab 140413, India

[4] Department of Sustainable Engineering, Saveetha School of Engineering, SIMATS, Chennai, Tamil Nadu 602105, India

public health (Heydari et al. 2020; Kotzias 2022). Benzene, a monocyclic aromatic hydrocarbon, is a notable toxic solvent in Group 1A. It is highly reactive in atmospheric photochemical reactions in which benzene has been well studied and can be carcinogenic depending on its concentration (IARC 2018). If the indoor premises are not adequately ventilated, heavy exposure to benzene in the air is associated with severe toxic effects, especially directly harmful to infants and children (Jia et al. 2019; Gabriel et al. 2021).

Since benzene has a broad spectrum of use, it is frequently used in areas such as producing furniture, wooden materials, and various solvent mixtures (Missia et al. 2010; Ruiz-Jimenez et al. 2022). Although the search for an alternative that can be used instead of benzene continues, it is frequently preferred under market conditions. Generally used in liquid form, benzene releases easily at room temperatures (20–25 °C). However, its chemically solid character is due to it not being easily oxidized and mineralized by oxygen underneath ambient conditions (Xie et al. 2020). Since the products used are indoor products, they mix with the indoor air very quickly. In this context, it negatively affects the indoor air and causes various health problems in humans depending on the exposure-concentration relationship. This wide variability in indoor air benzene presence emphasizes that its concentrations of about 1 to 250 µg/m^3, based on literature data, while its concentration limit of 5 µg/m^3 for the ambient atmospheric concentrations and 1.6 mg/m^3 for 8 h by European Directive 2008/50/EC (2008) and American Conference of Governmental Industrial Hygienists (ACGIH 1995). The evaluation result shows that these benzene concentrations are significantly higher than EU limitations (Lucialli et al. 2020; Wickliffe et al. 2020). For this purpose, benzene removal is an important issue, as it is a precursor toxic volatile organic substance to be removed from indoor air.

Such difficulty was due mainly to insufficient removal procedures for gas-phase benzene capture. Many studies have aimed to eliminate it, and various methods have been used to reduce exposure (Mishra and Mohanty 2022). Among these, the adsorption tool has a high rate of benzene removal, and although various types of adsorbents are used, activated carbon has achieved success in terms of performance/cost. The adsorption of benzene in several case studies likewise has fallen off drastically, with the adsorbed benzene amount decreased by 30 to 95% of initial concentrations (Zhang et al. 2023). The adsorbent quality, surface area, micropore volume, and amount are essential in benzene adsorption.

However, the lack of increased efficiency of benzene capturing does not provide a sufficient indicator basis for micropore volume (Isinkaralar 2023a). The authors also discussed confounding variables for multi-component or single-component benzene adsorption efficiency (Zhang et al. 2024). However, all of them provided the results of gas adsorption onto activated carbon, which is novel, and synthesis from diverse waste will no doubt provide the substance for diverse materials. Traditionally, renewable, inexpensive precursors, algae (Amarasekara et al. 2017), coconut shells (Vilella et al. 2017), corn cob and red mombin seed (Cruz et al. 2018), peach stone (Tsoncheva et al. 2018), cassava (Pongener et al. 2018), *Petai Belalang* tree (Wan Ibrahim et al. 2019), mango seed (Dzigbor and Chimphango 2019), and *Pterocladia capillacea* (Shoaib et al. 2020) are used to assess the physical or chemical of production in carbonaceous material (Serafin et al.2017). The activated carbon production involving a wide variety of proposed waste lignin biomass (Ibeh et al. 2019), a low-cost, environmentally friendly method (Hoang et al. 2022), has been produced and occasionally leads to complete failure of the not produced appropriately effective adsorbent (Querejeta et al. 2018; Boundzanga et al. 2020). Since the waste used cannot be disposed of at present, recycling contributes to the country's economy (Potbhare et al. 2019; Chouke et al. 2022). Some researchers have suggested that benzene vapor adsorption onto activated carbon has been the subject of recent investigations to examine the relationship between benzene molecules and adsorption behaviors (Isinkaralar 2024). This waste seems to be particularly appropriate for the production of activated carbon. *Heracleum platytaenium* Boiss. (Cow parsnip) is a typically desirable biomass in the forest. It is widely found in nature and grows abundantly on its own, and when it dries at the end of the season, it ends up as biomass waste in its environment. These plants are discarded and hence remain a significant disposal challenge when it dries up.

Heracleum platytaenium Boiss. (Cow parsnip) precursor (HPB) has traditionally been utilized for a variety of applications and then becomes waste after use. Waste biomass that is readily and abundantly available was synthesized as the optimal carbon adsorbent using chemical activation techniques via sodium hydroxide (NaOH). A batch adsorption system with novel HPB-derived carbonaceous material (HPAC) samples was performed for the benzene capture application in the gas phase. The HPACs were adequately characterized by Brunauer–Emmett–Teller (BET), N_2 adsorption–desorption, thermogravimetric (TG), Fourier transform infrared spectroscopy (FTIR), laser Raman spectrophotometer, and scanning electron microscopy (SEM). The adsorption capacities of several HPACs from benzene vapor were studied, which has become an attractive strategy for a solid binding force of benzene molecules. This paper not only reveals excellent perspectives for the treatment of benzene molecules but also indicates the application prospects of HPACs for indoor air pollution control.

Materials and methods

Materials and reagents

Heracleum platytaenium Boiss. (Cow parsnip) was collected from Kastamonu province, washed with distilled water, and oven-dried at 65 °C for 72 h to consume moisture. Then, the residue of biomass was grounded and sieved with 60-mesh. The sodium hydroxide (NaOH, purity ≥ 96%) and benzene (purity ≥ 99.5%) were purchased from Sigma-Aldrich. The reagents were analytical grade and have not been further purified. Milli-Q water was used throughout the experiment.

Preparation of porous carbons

A one-step procedure was applied: carbonization (varying from 500 to 900 °C, exploiting a 10 °C/min^{-1} heating rate) with chemical activation (activating agent: NaOH). The saturated solution of NaOH was recruited for the wet impregnation of the precursor stirred by a magnetic follower at 75 °C for 100 min. The mass ratio of dry biomass blended with NaOH was identical to 1:4 until the paste mixture. Afterward, it was dried in the oven at 105 °C for 48 h and carbonized at 500, 600, 700, 800, and 900 °C for 90 min under nitrogen (N_2) flow at a flow rate of 70 mL/min. After carbonization, the activated carbon sample (HPAC) was rinsed several times with deionized water, soaked in 0.2 M HCl, and subsequently washed with water so the final filtered water was not acidic. The N_2 stream was also used during the cooling stage. Eventually, the samples were oven-dried at 200 °C for 12 h. The efficiency of the obtained HPACs was measured as a percentage and calculated according to Eq. (1):

$$\text{Yield } \% : \frac{\text{Weight}_{\text{HPACs}}}{\text{Weight}_{\text{HPB}}} \times 100 \quad (1)$$

Analytical procedures and characterizations

Analytical procedures and characterizations are present in Fig. 1. HPACs were characterized using a QuantaTM 250 FEG scanning electron microscope (SEM) to scrutinize the morphological properties of the samples' surface at 10,000 × magnification. The Brunauer–Emmett–Teller (BET) and density functional theory (DFT) methods were used to evaluate surface properties and porosities through the chemisorption–physisorption analyzer model Autosorb-1-C (Quantachrome Instruments). EuroVector's EA3000 elemental analyzer detected the elemental compositions of the raw HPB and HPACs, according to ASTM D5291-96. The Raman spectra of the samples were investigated using Jasco NRS-4500 spectroscopy suite software. The FTIR spectra were acquired using a PerkinElmer Spectrum100 FTIR spectrophotometer, employing the KBr pellet method, within the frequency range of 400–4000 cm^{-1} and a resolution of 4 cm^{-1} with 32 scans. For the thermal analysis of the biomass, the Shimadzu DTG-60H model thermal analyzer was used with a heating rate of 10 ºC/min starting from 25 up to 600 °C in an inert atmosphere with a flow rate of 50 mL/min. A temperature of 500 °C is the maximum suggested temperature for chemical activation with acid-activating agents, and therefore, a maximum temperature of 600 °C was selected for the thermal analysis.

Design of benzene sorption

To determine the adsorption capability of HPACs, including HPAC500, HPAC600, HPAC700, HPAC800, and HPAC900, batch adsorption treatment was conducted using a gaseous benzene tank. Benzene vapor has occurred at temperatures (25 and 35 °C) and was investigated under such contact time (1–60 min), initial level (5–200 mg/L), and relative humidity (20 and 80%RH). Each HPAC was used 0.1 g and collected to Tenax®-TA sorbent tubes via chromatography/mass spectrometry detector (Thermo Scientific Trace 1300 gas), and all tubes were evaluated with the US EPA TO-17 Method (USEPA 1999). The benzene adsorption capacities were obtained by determining Eq. (2) which C_i (mg/L) and C_o (mg/L) refer to the benzene content at equilibrium condition; in addition, the feeder flux rate (F) of 85 mL/min and 0.1 g of HPACs (W) were exploited for applied adsorption reactions.

$$q_{(mg/g)} = \left(\frac{F \times C_0 \times 10^{-9}}{W}\right)\left[\left(\frac{C_i}{C_0} \times t_s\right) - \left(\int_0^{t_s} \frac{C_i}{C_0} \mathrm{d}_t\right)\right] \quad (2)$$

Adsorption kinetic

Adsorption kinetic is vital for assessing the procedure and effectiveness of the adsorption method. Pseudo-first-order (PFOM) and pseudo-second-order (PSOM) models are used to determine the adsorption kinetic data Eqs. 3 and 4, respectively, as stated by Sophia and Lima (2018).

$$q_t : q_e\left(1 - e^{-k_1 t}\right) \quad (3)$$

$$q_t : \frac{k_2 q_e t}{1 + k_2 q_e t} \quad (4)$$

K_1 is the PFOM unit constant, and K_2 is the PSOM rate constant, where qt and qe are the amounts of benzene adsorption at a specific equilibrium and time t (in mg/g).

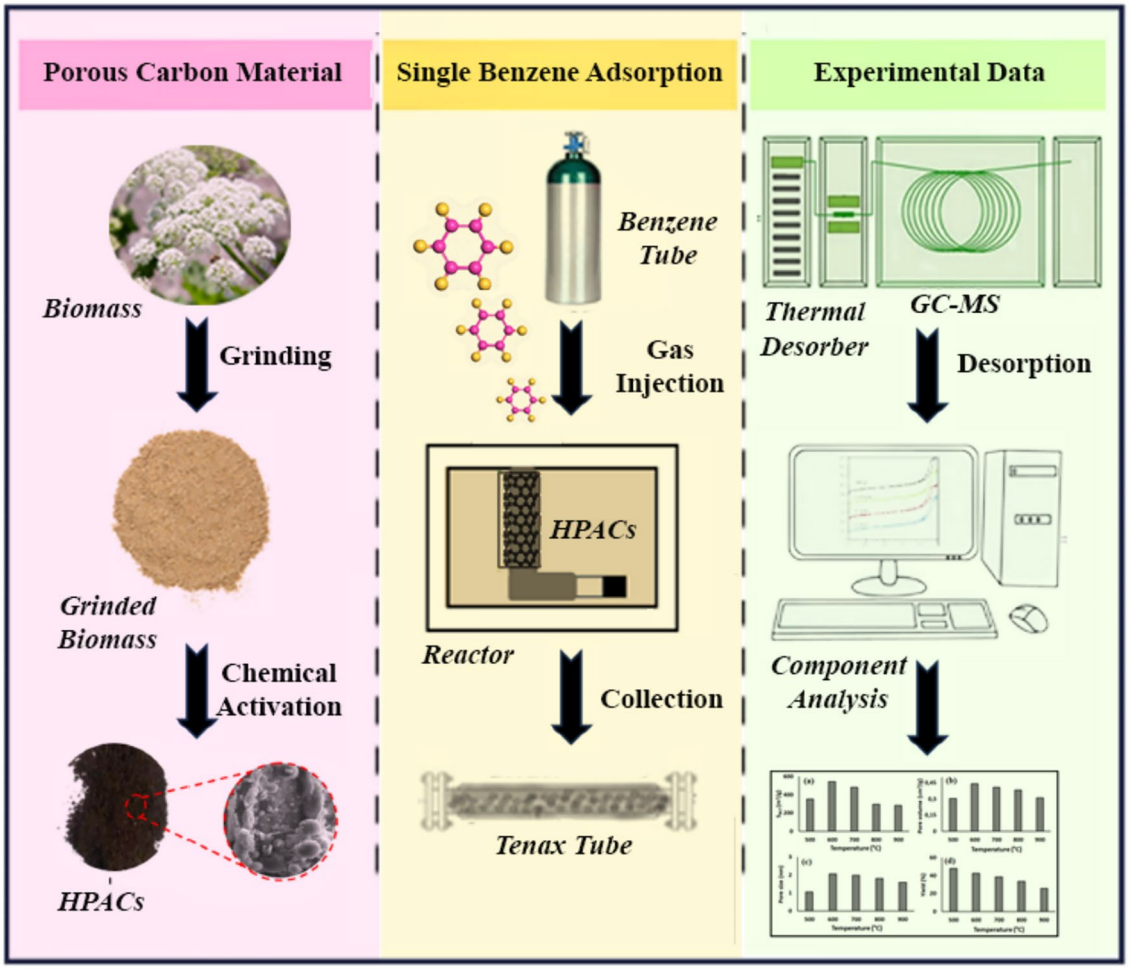

Fig. 1 Schematic representation of synthesis activated carbon and gaseous benzene adsorption

Adsorption isotherm

Adsorption isotherm provides an understanding of how benzene molecules follow and interrelate with the surface of a solid substance. In this research, for the HPAC600 to effectively eliminate benzene, isotherm models were used to match the adsorption information. The Langmuir isotherm model is applicable for monolayer adsorption onto surfaces with a limited number of identical sites (Zheng et al. 2008) and is expressed below in a linearized version Eq. (5) and the Freundlich model described the connection among the concentration, K and $1/n$ equilibrium constants. It is expressed in the nonlinear equation below in Eq. (6).

$$q_e : \frac{q_m \times K_L \times C_e}{1 + K_L C_e} \tag{5}$$

$$q_e : K \times C_e^{1/n} \tag{6}$$

where q_e is the quantity of benzene at equilibrium adsorbed (mg g^{-1}), C_e is the amount of benzene in the mixture at equilibrium (mg L^{-1}), q_{max}: monolayer rate of adsorbent (mg g^{-1}), and K_L (L mg $^{-1}$) is the Langmuir constant, which is linked to adsorption energy.

Results and discussion

The purpose of the research was to generate HPACs from HPB, and the results obtained from the test and characterization are mainly presented in several analyses.

Elemental analysis

Elemental analysis enables the identification of carbon (C), hydrogen (H), nitrogen (N), and sulfur (S) that occur in the HPACs. The HPACs were examined for elemental analysis in Table 1, and it was seen that the C content decreased from 86.3 to 61.3% after activation with NaOH. It was observed

Table 1 Elemental analysis of HPACs

Sampling ID	C (%)	N (%)	H (%)	S (%)	O (%)
HPB	86.3	2.5	4.7	0.8	5.7
HPAC500	78.7	2.1	2.9	0.5	15.8
HPAC600	73.5	1.9	3.2	0.9	20.5
HPAC700	70.1	1.5	3.4	1.2	23.8
HPAC800	64.9	4.2	4.8	5.3	20.8
HPAC900	61.3	3.1	5.2	3.7	23.7

that as the mass ratio of NaOH to biomass increased, the O content increased from 5.7 to 23.7%; the increase in oxygen content indicates a contribution to the absorption of acidic gases. Consistent with this observation is the idea that O entry happens during the activation process containing NaOH. The O-containing structures in HPACs behave like basic functional groups; such functional groups might be absorbing acidic gases. HPAC900 has a higher number of basic regions, and the percentage of C content (%) decreased with increasing carbonization temperature and was lowest for HPAC900 (61.3%), probably due to the removal of C–C bonds in contrast to oxygen functions. The increased oxygen component suggests that the activation process contributes oxygen molecules to the adsorbent. The decrease in the elemental percentages of C, H, N, and S in HPACs can be related to the deletion of elements. Furthermore, the presence of oxygen functional groups that display basic features may facilitate acid–base reactions, thereby improving gaseous benzene capture activity. Results show a good correlation with the results obtained analyzing the surface area.

Characteristics of the HPACs

Less loss is a desirable advantage in producing HPACs, leading to acquiring more samples. Hence, the parameters influencing the production yield, like the carbonization temperature and the pyrolyzing time, are adequate and should be controlled in Fig. 2.

Such influences during pyrolysis can change the final product yield between 25.8 and 48.1%. Nevertheless, HPAC500, HPAC600, HPAC700, HPAC800, and HPAC900 were subjected to surface analyses, and since they were of high micro, total pore volumes, and yield in Table 2, these samples were exploited for benzene sorption experiments. However, the HPAC600 had the highest surface area and micropore volume, with 543 m^2/g and 0.354 cm^3/g. The investigation revealed that the HPACs exhibited a range of surface areas, specifically within the 283–543 m^2/g range. Additionally, the micropore volume experienced an increase from 0.213 to 0.554 cm^3/g, as determined by analyzing the textural features of the HPAC500 to HPAC900. The total pore volume, micropores, and specific surface area results were consistent with the values reported in the literature by

Table 2 The pore structures of HPACs

Samples	S_{BET} (m^2/g)	V_{micro} (cm^3/g)	V_{total} (cm^3/g)
HPAC500	352 ± 18.7	0.259 ± 0.008	0.304 ± 0.18
HPAC600	543 ± 36.9	0.354 ± 0.015	0.642 ± 0.23
HPAC700	481 ± 40.1	0.327 ± 0.029	0.707 ± 0.19
HPAC800	298 ± 58.2	0.286 ± 0.033	0.384 ± 0.33
HPAC900	283 ± 50.8	0.213 ± 0.017	0.309 ± 0.27

Results are presented as average ± standard deviation of analysis of triplicate samples; S_{BET} (m^2/g): The BET specific surface area; V_{micro} (cm^3/g): Micro is the micropore volume; V_{total} (cm^3/g): The total pore volume.

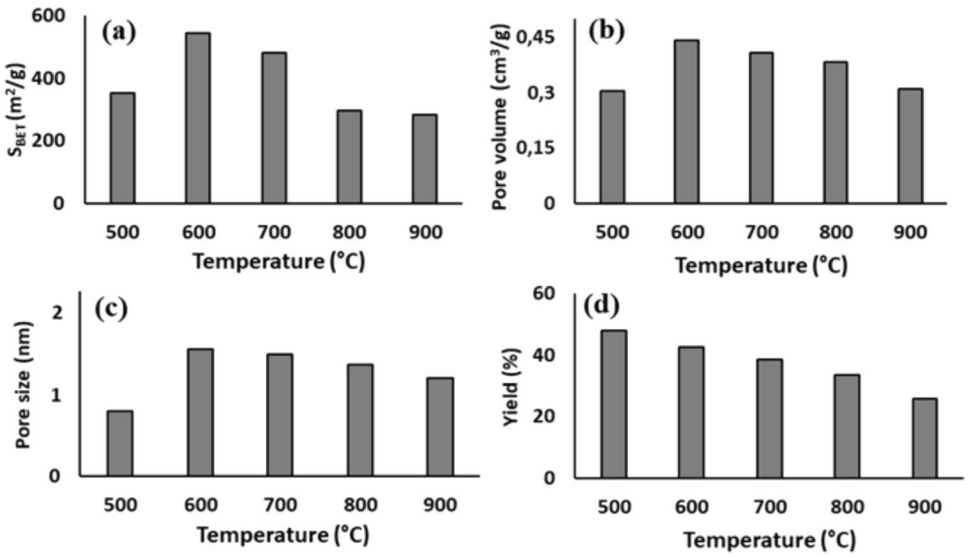

Fig. 2 Effect of carbonization temperature on surface area **a**, pore volume **b**, pore size **c**, and yield **d** of HPACs

Qiang et al. (2016) and Sun et al. (2022). Similarly reported by Islam et al. (2017) and Foo and Hameed (2012), prepared HAC from biomass shows that better surface area and pore volume were 1135 m^2/g and 0.60 cm^3/g, JPAC from jackfruit peel investigated that surface area and pore volume were 1286.70 m^2/g and 0.764 cm^3/g, respectively.

The N_2 adsorption–desorption method was used to investigate the surface area and pore size distribution of HPAC500, HPAC600, HPAC700, HPAC800, and HPAC900. Figure 3 presents the nitrogen adsorption–desorption isotherms of the PAC500, HPAC600, HPAC700, HPAC800, and HPAC900 at relative pressures $P/P_0 < 0.1$, indicating a significant number of mesoporous. This conclusion is supported by the fact that HPAC600 and HPAC700 exhibited type IV characteristics. At the same time, PAC500, HPAC800, and HPAC900 presented type I as per the International Union of Pure and Applied Chemistry (IUPAC 1994) classification (Lin et al. 2015; Li et al. 2018). At the relative pressure P/P_0 less than 0.2, the adsorption amount rapidly enhances with the increase in relative pressure, and the adsorption rate is quick except for HPAC500. The adsorption capacity keeps going up with the increase in the relative pressure, excluding HPAC900 and HPAC800, but growth tendency decreases at HPAC700 and HPAC600. Because of HPAC700 and HPAC600 have a large number of mesopores and macropores, it showed an obvious hysteresis loop. If the relative pressure reaches 1.0, the adsorption capacity of the macropores sharply increases due to capillary condensation (Li et al. 2022). Due to this capillary condensation, a meniscus emerges in the pores of the HPACs. Adsorption isotherm does not interfere with the desorption isotherm when adsorbate desorbs, giving rise to a hysteresis loop (Quan et al. 2020).

Figure 4 is the FTIR pattern of HPB and HPACs with NaOH chemical activators, which could be revealed and depicted for common bands at 3444, 2954, 1711, 1478, 1080, and 902 cm^{-1}. The FTIR spectrum of the HPAC500, HPAC600, HPAC700, HPAC800, and HPAC900 comprised of several absorption peaks, corresponding to O–H vibrations of cellulose, pectin, absorbed water, hemicellulose, and lignin (phenolic groups at 3444 cm^{-1}), dehydration and elimination reactions that release volatile products such as water, acetic acid, methanol, and furan derivatives (Pallarés et al. 2018; Valencia et al. 2022), asymmetric C–H stretching (2954 cm^{-1}) in CH_3 group (Wei et al. 2023), C=O stretching (slight 1711 cm^{-1}) (Freitas et al. 2019), and O–C–O stretching in the lignocellulosic (1080 cm^{-1}) (Tang et al. 2023), whereas those of C=C and C–O stretching stayed with the emergence of C–H bending (absorption peaks at 1478 cm^{-1}) (Isinkaralar 2023b) and C=C bending (weak bonds at 902 cm^{-1}) (Serafin et al. 2019). The band intensity observed at 1711 cm^{-1} is higher for HPAC900, indicating the presence of C=O functional groups in the fabricated material (Saleh 2018; Mishra and Mohanty 2021).

Figure 5 displays the HPACs Raman spectral data of the HPAC500, HPAC600, HPAC700, HPAC800, and HPAC900. The bands detected at wavenumbers 1308 cm^{-1} and 1571 cm^{-1} represent the D and G band stretching vibration of the sp^2-hybridized graphitic carbon atoms in the aromatic hexagonal sheet (Ferrari and Robertson 2000). Also, D band reflects lattice structures with the E_{2g} symmetry and vacancies in aromatic ring lamellae (Sadezky et al. 2005). Whereas the G band in graphite is widely thought to be due to in-plane C–C stretching vibrations of the graphite layers, the D band is ascribed to structural defects inside the graphite material (Senthilkumar et al. 2011). Among the carbon

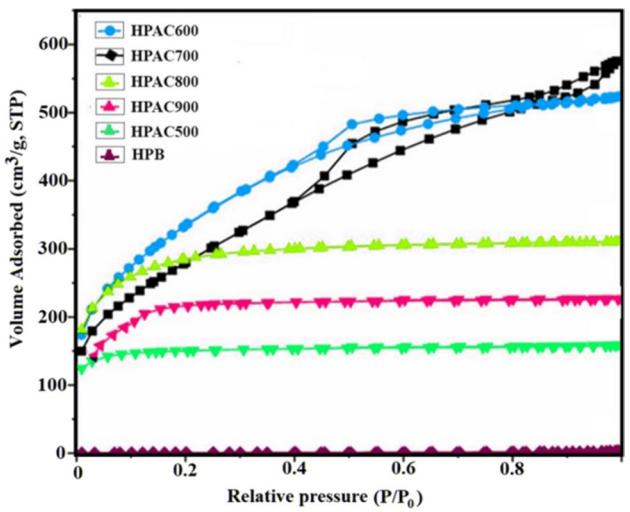

Fig. 3 N_2 adsorption–desorption of isotherms of HPACs

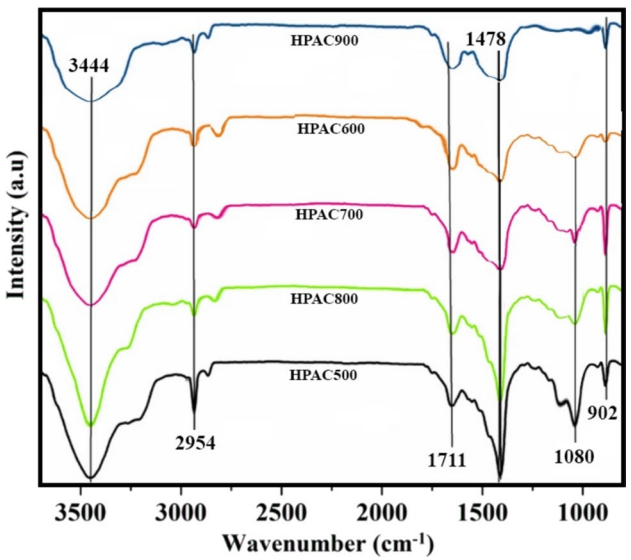

Fig. 4 FTIR spectra of HPACs

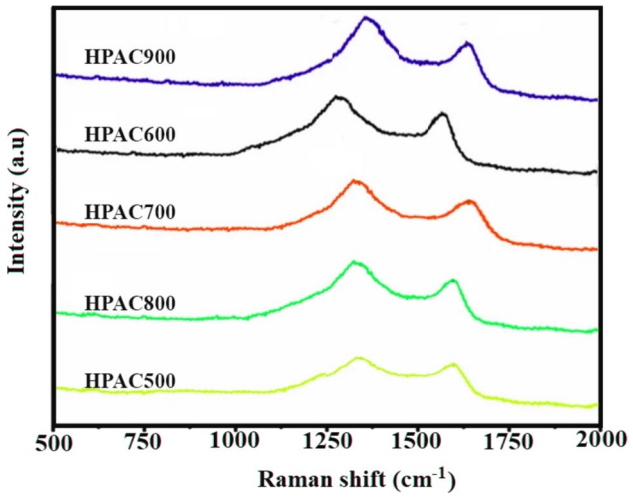

Fig. 5 Raman spectra of HPACs

materials, the *R* values of HPAC500, HPAC600, HPAC700, HPAC800, and HPAC900 are 2.08, 2.66, 2.34, 2.19, and 3.02, respectively. Our studies show that HPAC500 has the greatest graphitization level compared to the reported peak position (Sonkusare et al. 2020), followed by HPAC800, HPAC700, HPAC600, and HPAC900.

Figure 6 shows the thermogravimetric analysis results of HPACs and HPB and represents the materials' thermal decomposition stages. The HPB and HPACs exhibited distinct performances during pyrolysis. Thermal decomposition steps varied dramatically between the biomasses due to their different chemical compositions, particularly their extractive ingredients. The HPB is a lignocellulosic biomass material composed of cellulose, hemicellulose, and lignin, eliminating moisture, devolatilization, and decomposition. The natural humidity mass loss of about 8.5% was recorded as a critical weight loss up to 190 °C, and in the second stage, a significant change in mass loss of about 45% was observed with sharp peaks in the 390 °C temperature range. Decomposition of hemicellulose and lignin in HPB was induced mass reduction beyond 350 °C. The carbonization temperature range considered was 420 °C for the study, and the weight loss became very slow after this temperature. Similarly, Xu et al. (2010) investigated that lignin decomposition in raw material decomposes at last, contributing to carbon formation. In the thermal decomposition of two seeds, according to Maia et al. (2021), three distinct regions of mass loss presenting a drastic weight loss exist, referring to the following phenomena: dehydration, active pyrolysis, and passive pyrolysis or carbonization of the present work. The first decomposition is attributed to the evaporation of humidity. It is recognizable that HPAC500 deteriorated more rapidly than HPAC900. Several research studies proposed that mass loss mainly depends on carbonization temperature, such as Rovani et al. (2016), Pathak et al. (2015), and Habeeb et al. (2020). In HPAC500, this is illustrated by the fact that at around 230 °C, there is a rapid weight loss of the material. In contrast, in HPAC900, the mass loss starts at approximately 340 °C, which demonstrates the thermal stability of 900 °C compared to 500 °C.

Figure 7 demonstrates the scanning electron microscopy (SEM) forms of HPB, HPAC500, HPAC600, HPAC700, HPAC800, and HPAC900, which SEM revealed at a

Fig. 6 TG curve of HPACs

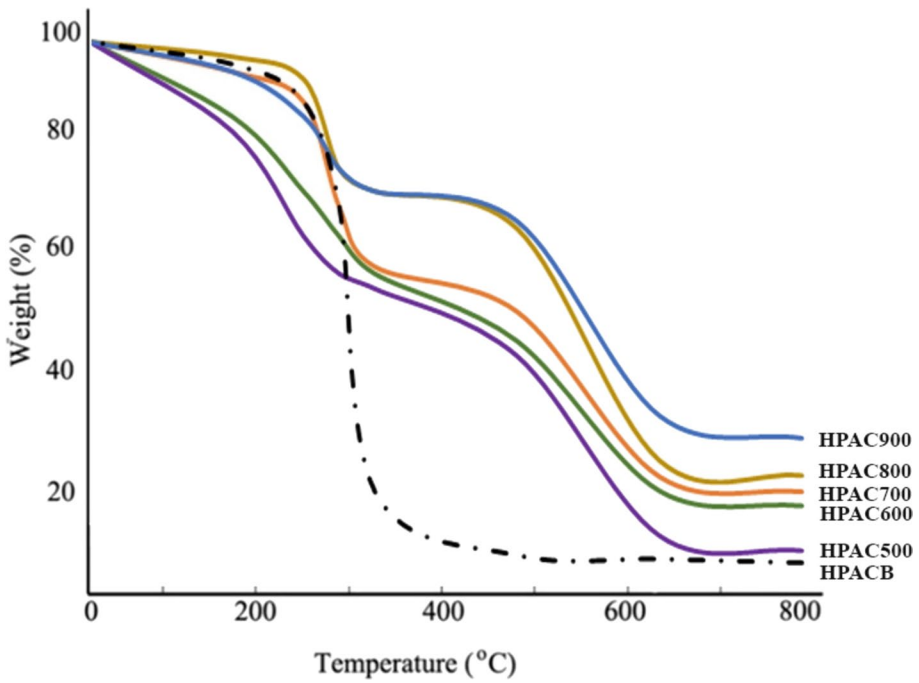

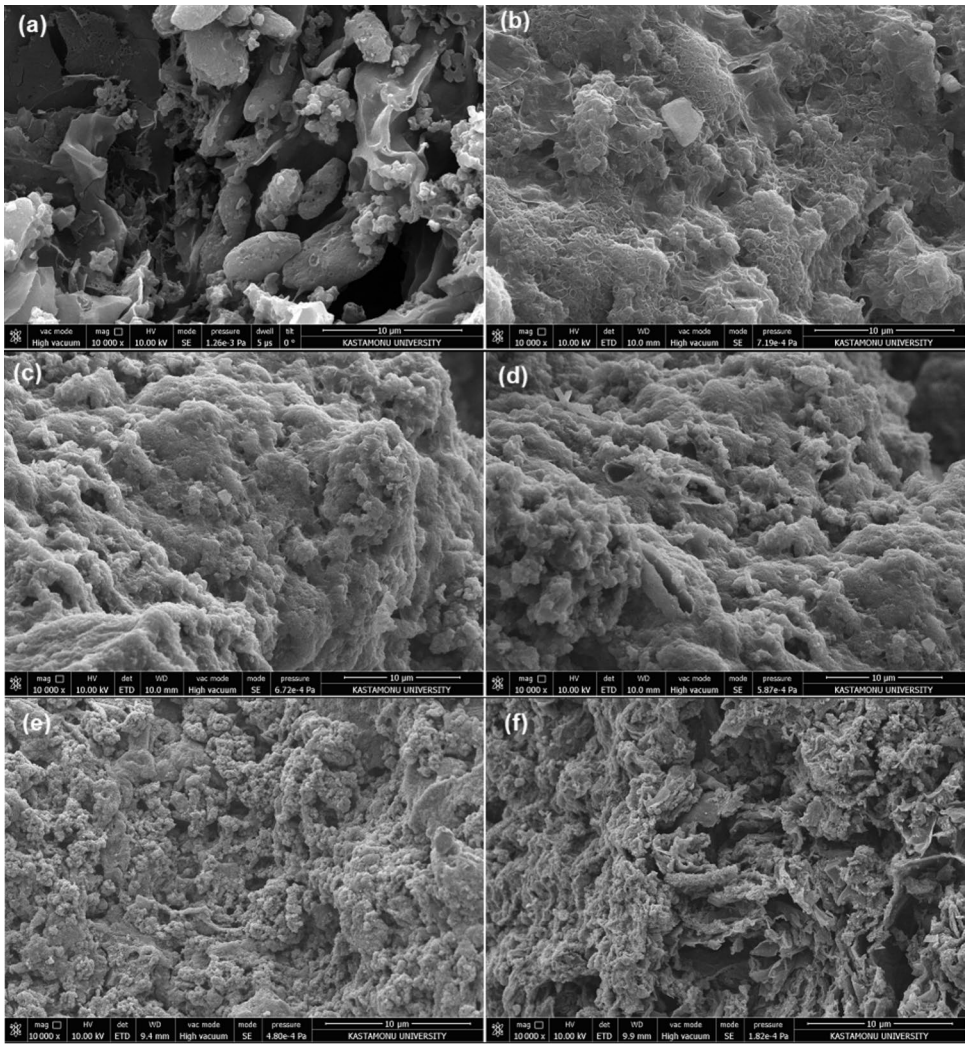

Fig. 7 Scanning electron micrographs × 10,000 magnitude: **a** HPB; **b** HPAC500; **c** HPAC600; **d** HPAC700; **e** HPAC800; and **f** HPAC900

magnification scale of 10,000x. The HPB showed an irregular structure and inhomogeneous surface with niggardly small cavities on the bieads, while NaOH activating caused an irregular and heterogeneous surface morphology with a well-developed porous structure. The HPAC500, HPAC600, and HPAC700 have relatively small sizes of spherical particles; however, HPAC800 and HPAC900 revealed micro and nanostructured carbon particles network-like spherical-shape formation. The HPB has a negligible number of pores, although HPAC500, HPAC600, HPAC700, HPAC800, and HPAC900 can demonstrate cracks, crevices, and large grains of different sizes (Correa et al. 2017). The structures formed after activation and pyrolysis processes were seen to become numerous distributed pores. Similar surface morphology of the activated materials presents irregular but highly porous surface structure SEM micrographs by Ahmed et al. (2019) and Aloud et al. (2023). In general, the higher calcination temperature damaged the evolution of micropore domains due to the shrinkage influence on carbon microstructures, and porosity manifested itself in these nanostructures (Muniandy et al. 2014; Rois et al. 2021; Isinkaralar et al. 2022).

Mechanism of benzene adsorption onto HPACs

The experimental apparatus was then permitted to attain a stabilization state condition before starting the tests as shown in Fig. 8. The humidity was adjusted to be close to average room conditions and measured 65 ± 2%. The concentration was gradually increased with increasing benzene molecules attached to the adsorbent surface. The trend line of the curves as shown in Fig. 8a was formed at 25 °C, and it was observed that HPAC700 was faster than the others in the first moments (117 mg/g) but reached saturation capacity early with increasing benzene amounts. The adsorption capacity of HPAC600 (127 mg/g) was higher than the others, and it was determined that it reached constant conditions for a longer time. HPAC500, HPAC800, and HPAC900 adsorption capacities were 80, 101, and 59 mg/g, respectively. In Fig. 8b, the ambient temperature increased to 35 °C. The

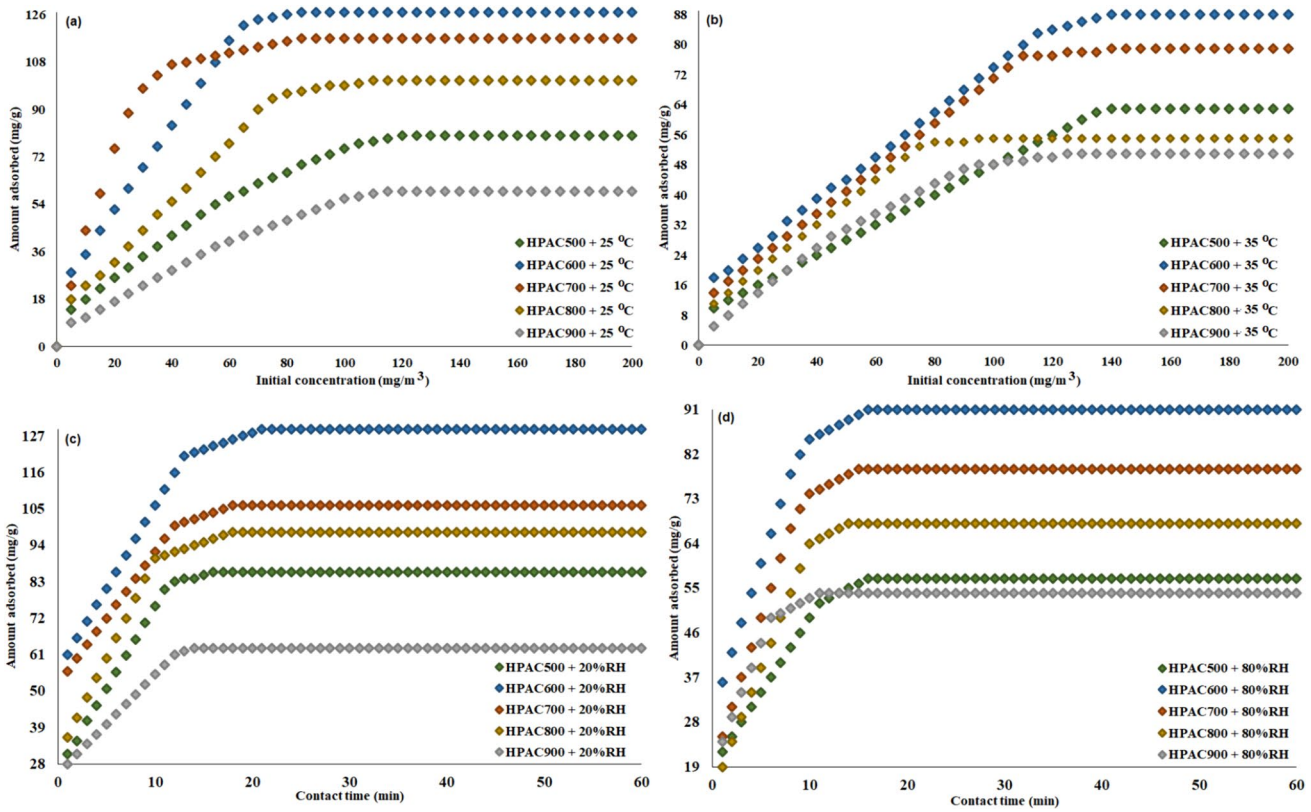

Fig. 8 Benzene sorption capacities of HPACs: **a** 25 °C, **b** 35 °C, **c** 20%RH, and d 80RH%

adsorption capacity (88 mg/g) and capture rate of HPAC600 were higher than the others, but the adsorption capacity (55 mg/g) of HPAC800 was significantly decreased compared to that at 25 °C. HPAC500, HPAC700, and HPAC900 adsorption capacities were 63, 79, and 51 mg/g, respectively. Keeping the operating conditions constant, the percentage decreases in adsorption capacity for HPAC500, HPAC600, HPAC700, HPAC800, and HPAC900 for an increase of only 10 °C were calculated as 21, 31, 32, 46, and 14%, respectively. Although HPAC800 showed the highest yield decrease, HPAC900 showed the lowest yield decrease. The main reason may be that the microporosity is lower than the others.

In the studies in Fig. 8c and d, the concentration amount was injected as 200 mg/m^3, and the adsorption capacities were examined according to the waiting time. The main difference here is that the average moisture content was changed, and the moisture content was reduced to 20% in Fig. 8c but increased to 80% in Fig. 8d. Although an increase in adsorption capacities was detected in Fig. 8c, a decrease was determined in the slope line as shown in Fig. 8d. In Fig. 8c, the adsorption capacities for HPAC500, HPAC600, HPAC700, HPAC800, and HPAC900 were 86, 129, 106, 98, and 63 mg/g, respectively, whereas in Fig. 8d, these values were 57, 91, 79, 68, and 54 mg/g, respectively. Keeping the operating conditions constant, the percentage decreases in adsorption capacity on HPAC500, HPAC600, HPAC700, HPAC800, and HPAC900 were calculated to be 34, 29, 25, 31, and 13%, respectively, when the moisture content was increased only from 20 to 80%. According to the results, in the first stage of benzene adsorption, the pores of each adsorbent sufficiently contained the benzene molecules. As the contact time increased, the adsorption process gradually approached saturation.

Although HPAC500 showed the highest yield decrease, HPAC900 showed the lowest yield decrease. The main reason for this is that the microporosity of HPAC900 is lower than the others, and it cannot capture benzene molecules. It indicates that the micropore performance increases, and the pores are more open to capture. In considering micropore volume and total surface area, benzene adsorption capacities are HPAC600 > HPAC700 > HPAC800 > HPAC500 > HPAC 900 at different conditions.

Although various studies on gas adsorption are widespread, removal with adsorbents produced from lignin-based biomass wastes is relatively limited (Lv et al. 2020; Rajabi et al. 2021). Moreover, the difference in the gases removed, the diversity of adsorbents used, and variations in application methods and inputs in the process lead to differentiation in adsorption (Ukanwa et al. 2019; Jareteg et al. 2021). Many

studies have observed that although the concentration and temperature varied, the amount of moisture did not change. The increase in concentration was an additional load on the adsorbent and led to the premature filling of its pores. In parallel with this, the increase in temperature increases the pore occupancy rate (Pui et al. 2019). Temperature did not directly affect the adsorbent but caused a difference in the adsorption of the adsorbent. The adsorbents used are benzene gas, which is at the beginning of VOCs and is perhaps the most challenging group to study in gas adsorption (Chen et al. 2021). Temperature is the main parameter of benzene, which can increasing slope evaporate from room temperature to higher temperature. In addition, differences in the amount of moisture in the ambient conditions play an influential role in the efficiency of the adsorbent. It has been explained in the studies that the increase in the amount of moisture in room conditions rapidly fills the pores in the adsorbent, and there is no space for the adsorbent (Heeley-Hill et al. 2021; Lobato-Peralta et al. 2021). For this reason, when benzene adsorption studies are examined, temperature, concentration, and humidity amount come to the fore, while the adsorbent structure and adsorption setup used are also necessary (Maneerung et al.2016; Gabruś et al. 2022). Examining the single adsorption process is used to realize the significance of benzene molecules in equilibrium conditions. The concentrations of ACs can be lowered due to their manufacturing scheme, the process and equipment, and changes in ambient conditions (temperature, humidity, and installation). In other works, benzene control approaches are extensively employed when the technology is limited or unavailable.

Benzene adsorption kinetic and isotherm of HPAC600

Understanding of adsorption kinetics is required to accurately comprehend the process of rate-controlled mass transfer adsorption phenomenon of benzene molecules in a single phase via HPAC600 adsorbers in a designed batch adsorption system and possibly even to scale up for actual air treatment (Liu et al. 2021). Table 3 shows that the high R^2 values (≥ 0.950) suggest that the kinetic models should be useful to describe the adsorption kinetics of benzene onto HPAC600 and the better fitness of PFOM in terms of the compatibility between the experimental and predicted adsorption capacities. This result suggests that chemisorption controlled the surface assimilation of benzene on HPAC600. It is essential to understand the strong covalent bonds to maintain benzene compounds attached to the surface of the adsorbent as shown by Long et al. (2019) and Park et al. (2019). PSOM model simulates the benzene adsorption process (Takaya et al. 2016), although PFOM results demonstrate a significant discrepancy between the estimated and experimental adsorption capacities (qe) for for reversible reactions of benzene molecules (Vikrant et al. 2018) by the prevailing mechanisms and physicochemical characteristics of the HPAC600.

Figure 9 shows that Langmuir model results fitted the information with R^2: 0.978; however, Freundlich model successfully indicated monolayer adsorption as R^2: 1.00. Utilizing the values of C_e/q_e (slope and intercept) with Ce, the Langmuir and Freundlich constants are confuted to better fitting results (Fig. 9c) and Log qe with Log ce (Fig. 9d), respectively (Roy et al. 2018). Wang et al. (2015) investigated benzene vapor adsorption onto ordered mesoporous carbon (OMC, pore size 1.8–5 nm) and showed difficulty entering the pore channel of benzene molecules (> 100 nm). These results correspond to the previous studies pointed out that the isotherm data of benzene vapor adsorption on HPAC600 fit well with the Freundlich isotherm model (R^2 1.000) and Langmuir isotherm (0.978) models; it was concluded that the latter offered the best fit (Table 4).

Although many different approaches have been used for VOC adsorption that depends on the different phenomena and improves their adsorption capacities under all conditions, they characterized through various isotherms, which may be influenced by the type of material utilized (Ushiki et al. 2014; Zhang et al. 2018; Wu et al. 2022). Similarly, benzene adsorption on HPAC600 was shown to be better adapted to the Freundlich isotherm which is mainly owing to the high R^2 values (above 0.99). Laskar et al. (2019) studied simultaneous adsorption of VOCs onto beaded activated carbon (BAC), which significantly fitted the Manes method for polar VOCs. Similar experimental findings have also been reported by Saha et al. (2018) and Zhang et al. (2022) that benzene molecules can easily diffuse to the inner surfaces of

Table 3 Nonlinear PFOM and PSOM kinetic constants of benzene adsorption on the HPAC600

Experiment No	Ambient temperature	RH (%)	PFOM			PSOM		
			$q_{e(\exp)}$ (mg g^{-1})	K_1 (h^{-1})	R^2	$q_{e(\exp)}$ (mg g^{-1})	K_2 (g mg^{-1} h^{-1})	R^2
1	25	20	124	0.29	0.956	135	0.0048	0.835
2	25	80	114	0.23	0.989	123	0.0036	0.903
3	35	20	91	0.16	0.979	108	0.0042	0.924
4	35	80	62	0.19	0.999	75	0.0033	0.997

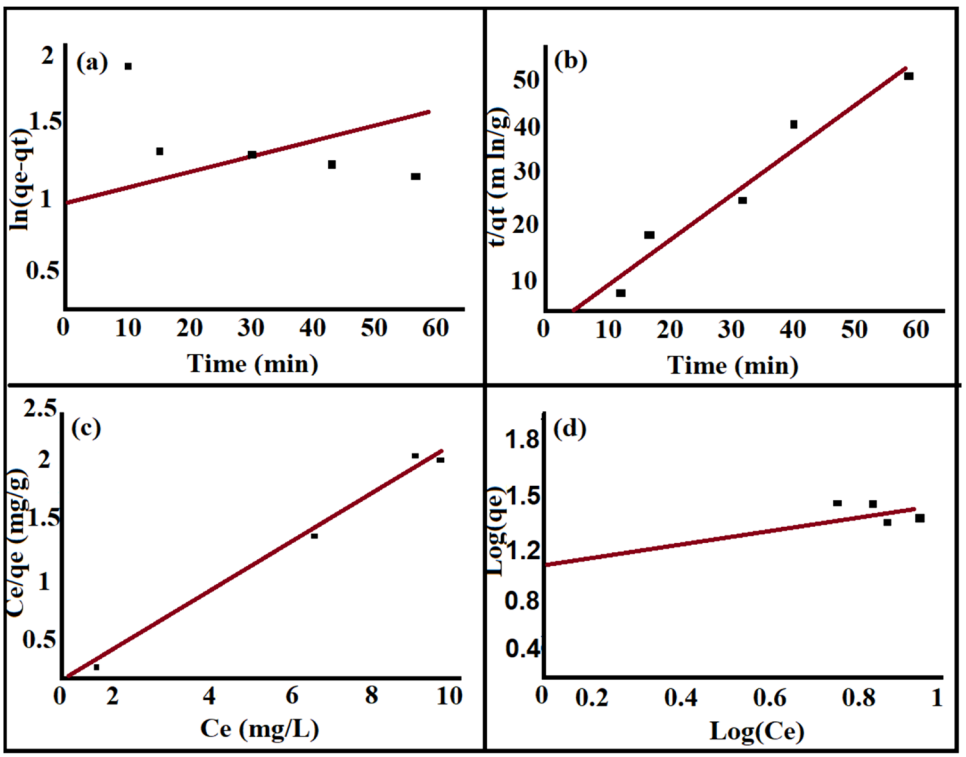

Fig. 9 Summary of **a** PFOM **b** PSOM, **c** Langmuir isotherm, and **d** Freundlich isotherm plots

Table 4 Nonlinear adsorption isotherm constants for Langmuir and Freundlich

RH (%)	Ambient temperature	Langmuir			Freundlich		
		q_e(mg g^{-1})	K_L	R^2	K_F (mg g^{-1})	n	R^2
20	25	127	0.6	0.962	53	3.3	0.985
	35	77	1.5	0.633	47	5.2	0.361
80	25	113	0.62	0.978	42	1.7	1.00
	35	98	1.1	0.929	56	5	0.695

the pores of HPAC600 and can be encouraged with increasing concentration and adsorption temperature.

Conclusions

Biomass-derived HPACs with benzene capture were trumphically fabricated via NaOH activation and carbonization. The HPB strongly affected the textural features of the attained carbon. HPAC600, with various micropore sizes, was the most influential sample for benzene sorption and exhibited different sensitivities to the treatment process, with temperatures and relative humidity. When the temperature was raised to 35 °C, the range of effective micropores for benzene adsorption at 80% RH declined to 13–46%. For the typical room conditions, the HPAC600 was mainly effective, with the highest sorbed quantity of benzene molecules equal to 127 mg/g. The HPAC600 can be utilized for various applications, such as flue gas and industrial emissions. Benzene adsorption onto HPAC600 suits PFOM data better; the information was effectively fitted by the Freundlich model. It indicates monolayer adsorption; however, more investigations on removing benzene molecules, especially employing this process, would benefit other VOCs. Also, to ensure the sustainability of the process, long-term demonstration projects are required that consider the impact of other gases on multi-component adsorption.

Acknowledgements Not applicable.

Authors' contribution Kaan Isinkaralar was contributed conceptualization, investigation, methodology, and writing—original draft. Aydin Turkyilmaz was involved in data curation and writing—review and editing. Ahmad Hosseini-Bandegharaei was performed methodology, validation, and writing—review and editing. Chander Prakash was done formal analysis and writing—review and editing.

Funding There is no financial support and commercial support.

Data availability The data that support the findings of this study are available from the corresponding author, upon reasonable request.

Declarations

Conflict of ınterest The authors declare that they have no conflict of interest.

Consent to participate Not applicable.

Consent to publish Not applicable.

Ethics approval All authors have read, understood, and have complied as applicable with the statement on "Ethical responsibilities of Authors" as found in the Instructions for Authors.

References

Adamović D, Dorić J, Vojinović-Miloradov M (2013) BTEX in the exhaust emissions of motor vehicles. Causes Impacts Solut Glob Warm. https://doi.org/10.1007/978-1-4614-7588-0_21

Ahmed MB, Johir MAH, Zhou JL, Ngo HH, Nghiem LD, Richardson C, Moni MA, Bryant MR (2019) Activated carbon preparation from biomass feedstock: clean production and carbon dioxide adsorption. J Clean Prod 225:405–413. https://doi.org/10.1016/j.jclepro.2019.03.342

Aloud SS, Alharbi HA, Hameed BH, Giesy JP, Almady SS, Alotaibi KD (2023) Production of activated carbon from date palm stones by hydrothermal carbonization and microwave assisted KOH/NaOH mixture activation for dye adsorption. Sci Rep 13(1):19064. https://doi.org/10.1038/s41598-023-45864-z

Amarasekara A, Tanzim FS, Asmatulu E (2017) Briquetting and carbonization of naturally grown algae biomass for low-cost fuel and activated carbon production. Fuel 208:612–617. https://doi.org/10.1016/j.fuel.2017.07.034

American Conference of Governmental Industrial Hygienists (ACGIH) (1995) Threshold limit values for chemical substances and physical agents and biological exposure indices

Arnold SM, Angerer J, Boogaard PJ, Hughes MF, O'Lone RB, Robison SH, Robert Schnatter A (2013) The use of biomonitoring data in exposure and human health risk assessment: benzene case study. Crit Rev Toxicol 43(2):119–153. https://doi.org/10.3109/10408444.2012.756455

Boundzanga HM, Cagnon B, Roulet M, de Persis S, Vautrin-Ul C, Bonnamy S (2020) Contributions of hemicellulose, cellulose, and lignin to the mass and the porous characteristics of activated carbons produced from biomass residues by phosphoric acid activation. Biomass Convers Biorefinery 12:3081–3096. https://doi.org/10.1007/s13399-020-00816-9

Chen Q, Xiao R, Lei X, Yu T, Mo J (2021) Experimental and modeling investigations on the adsorption behaviors of indoor volatile organic compounds in an in-situ thermally regenerated adsorption-board module. Build Environ 203:108065. https://doi.org/10.1016/j.buildenv.2021.108065

Chouke PB, Dadure KM, Potbhare AK, Bhusari GS, Mondal A, Chaudhary K, Singh V, Desimone MF, Chauhary RG, Masram DT (2022) Biosynthesized δ-Bi_2O_3 nanoparticles from Crinum viviparum flower extract for photocatalytic dye degradation and molecular docking. ACS Omega 7(24):20983–20993. https://doi.org/10.1021/acsomega.2c01745

Commission E (2008) Directive 2008/50/EC of the European parliament and of the council of 21 May 2008 on ambient air quality and cleaner air for Europe. Off J Eur Union 152:1–44

Correa CR, Otto T, Kruse A (2017) Influence of the biomass components on the pore formation of activated carbon. Biomass Bioenerg 97:53–64. https://doi.org/10.1016/j.biombioe.2016.12.017

Cruz GJF, Gómez MM, Solis JL, Rimaycuna J, Solis RL, Cruz JF, Rathnayake B, Keiski RL (2018) Composites of ZnO nanoparticles and biomass based activated carbon: adsorption, photocatalytic and antibacterial capacities. Water Sci Technol 2017(2):492–508. https://doi.org/10.2166/wst.2018.176

Dzigbor A, Chimphango A (2019) Production and optimization of NaCl-activated carbon from mango seed using response surface methodology. Biomass Convers Biorefinery 9:421–431. https://doi.org/10.1007/s13399-018-0361-3

Edokpayi JN, Alayande SO, Adetoro A, Odiyo JO (2020) The equilibrium, kinetics, and thermodynamics studies of the sorption of methylene blue from aqueous solution using pulverized raw macadamia nut shells. J Anal Method Chem. https://doi.org/10.1155/2020/8840666

Fang L, Norris C, Johnson K, Cui X, Sun J, Teng Y, Tian E, Xu W, Li Z, Mo J, Schauer JJ, Black M, Bergin M, Zhang J, Zhang Y (2019) Toxic volatile organic compounds in 20 homes in Shanghai: concentrations, inhalation health risks, and the impacts of household air cleaning. Build Environ 157:309–318. https://doi.org/10.1016/j.buildenv.2019.04.047

Ferrari AC, Robertson J (2000) Interpretation of Raman spectra of disordered and amorphous carbon. Phys Rev B 61(20):14095. https://doi.org/10.1103/PhysRevB.61.14095

Fiebelkorn S, Meredith C (2018) Estimation of the leukemia risk in human populations exposed to benzene from tobacco smoke using epidemiological data. Risk Anal 38(7):1490–1501. https://doi.org/10.1111/risa.12956

Foo KY, Hameed BH (2012) Potential of jackfruit peel as precursor for activated carbon prepared by microwave induced NaOH activation. Bioresour Technol 112:143–150. https://doi.org/10.1016/j.biortech.2012.01.178

Freitas JV, Nogueira FG, Farinas CS (2019) Coconut shell activated carbon as an alternative adsorbent of inhibitors from lignocellulosic biomass pretreatment. Ind Crops Prod 137:16–23. https://doi.org/10.1016/j.indcrop.2019.05.018

Gabriel MF, Felgueiras F, Batista R, Ribeiro C, Ramos E, Mourão Z, de Oliveira FE (2021) Indoor environmental quality in households of families with infant twins under 1 year of age living in Porto. Environ Res 198:110477. https://doi.org/10.1016/j.envres.2020.110477

Gabruś E, Tabero P, Aleksandrzak T (2022) A study of the thermal regeneration of carbon and zeolite adsorbents after adsorption of 1-hexene vapor. Appl Therm Eng 216:119065. https://doi.org/10.1016/j.applthermaleng.2022.119065

Habeeb OA, Kanthasamy R, Saber SEM, Olalere OA (2020) Characterization of agriculture wastes based activated carbon for removal of hydrogen sulfide from petroleum refinery waste water. Mater Today Proc 20:588–594. https://doi.org/10.1016/j.matpr.2019.09.194

Heeley-Hill AC, Grange SK, Ward MW, Lewis AC, Owen N, Jordan C, Hodgson G, Adamson G (2021) Frequency of use of household products containing VOCs and indoor atmospheric concentrations in homes. Environ Sci Process Impacts 23(5):699–713. https://doi.org/10.1039/D0EM00504E

Heydari G, Ranjbar Vakilabadi D, Kermani M, Rayani M, Poureshgh Y, Behroozi M, Fanaei F, Arfaeinia H (2020) Load characteristics and inhalation risk assessment of benzene series (BTEX) pollutant in indoor air of Ghalyan and/or cigarette cafes compared to smoking-free cafes. Environ Pollut Bioavailab 32(1):26–35. https://doi.org/10.1080/26395940.2020.1713895

Hoang AT, Kumar S, Lichtfouse E, Cheng CK, Varma RS, Senthilkumar N, Nguyen PQP, Nguyen XP (2022) Remediation of heavy metal polluted waters using activated carbon from

lignocellulosic biomass: an update of recent trends. Chemosphere 302:134825. https://doi.org/10.1016/j.chemosphere.2022.134825

Ibeh PO, García-Mateos FJ, Rosas JM, Rodríguez-Mirasol J, Cordero T (2019) Activated carbon monoliths from lignocellulosic biomass waste for electrochemical applications. J Taiwan Inst Chem Eng 97:480–488. https://doi.org/10.1016/j.jtice.2019.02.019

International Agency for Research on Cancer (2018) IARC monographs on the evaluation of carcinogenic risks to humans 120 World Health Organization, Lyon, France

Isinkaralar K (2023a) Adsorption of gaseous naphthalene on carbonaceous sorbent: perspective of affecting factors. Biomass Convers Biorefinery. https://doi.org/10.1007/s13399-023-04755-z

Isinkaralar K (2023b) Optimal preparation of low-cost activated carbon: the enhanced mechanism of interaction and performance studies for volatile organic compounds (VOCs) capture. Biomass Convers Biorefinery. https://doi.org/10.1007/s13399-023-05159-9

Isinkaralar K (2024) Multi-component volatile organic compounds (VOCs) treatment nexus: High-performance of activated carbon derived from residual agroforestry biomass. Int J Environ Sci Technol 21(1):925–938. https://doi.org/10.1007/s13762-023-05202-2

Isinkaralar K, Gullu G, Turkyilmaz A, Dogan M, Turhan O (2022) Activated carbon production from horse chestnut shells for hydrogen storage. Int J Glob Warm 26(4):361–373. https://doi.org/10.1504/IJGW.2022.122430

Islam MA, Ahmed MJ, Khanday WA, Asif M, Hameed BH (2017) Mesoporous activated carbon prepared from NaOH activation of rattan (*Lacosperma secundiflorum*) hydrochar for methylene blue removal. Ecotoxicol Environ Saf 138:279–285. https://doi.org/10.1016/j.ecoenv.2017.01.010

IUPAC (1994) Recommendations for the characterization of porous solids. Pure Appl Chem 66(80):1739–1758

Jareteg A, Maggiolo D, Thunman H, Sasic S, Ström H (2021) Investigation of steam regeneration strategies for industrial-scale temperature-swing adsorption of benzene on activated carbon. Chem Eng Process-Process Intensif 167:108546. https://doi.org/10.1016/j.cep.2021.108546

Ji Y, Gao F, Wu Z, Li L, Li D, Zhang H, Zhang Y, Gao J, Bai Y, Li H (2020) A review of atmospheric benzene homologues in China: characterization, health risk assessment, source identification and countermeasures. J Environ Sci 95:225–239. https://doi.org/10.1016/j.jes.2020.03.035

Jia S, Sankaran G, Wang B, Shang H, Tan ST, Yap HM, Shen J, Gutiérrez RA, Fang W, Liu M, Chang VWC, Ng LC, Fang M (2019) Exposure and risk assessment of volatile organic compounds and airborne phthalates in Singapore's child care centers. Chemosphere 224:85–92. https://doi.org/10.1016/j.chemosphere.2019.02.120

Jiang L, Li Y, Cai Y, Liu K, Liu C, Zhang J (2022) Probabilistic health risk assessment and monetization based on benzene series exposure in newly renovated teaching buildings. Environ Int 163:107194. https://doi.org/10.1016/j.envint.2022.107194

Kotzias D (2022) Exposure to volatile organic compounds in indoor/outdoor environments and methodological approaches for exposure estimates-the European paradigm. J Hazard Mater Adv 8:100197. https://doi.org/10.1016/j.hazadv.2022.100197

Kozielska B, Kaleta D (2020) Assessment of indoor benzene and its alkyl derivatives concentrations in offices belonging to university of technology (Poland). Atmosphere 12(1):51. https://doi.org/10.3390/atmos12010051

Laskar II, Hashisho Z, Phillips JH, Anderson JE, Nichols M (2019) Competitive adsorption equilibrium modeling of volatile organic compound (VOC) and water vapor onto activated carbon. Sep Purif Technol 212:632–640. https://doi.org/10.1016/j.seppur.2018.11.073

Li S, Sun K, Shen Y, Li C, Li J (2018) Study on preparation of mandelium pedunculata husk-based mesoporous activated carbon by steam activation. Biomass Chem Eng 52(03):9–15. https://doi.org/10.3969/j.issn.1673-5854.2018.03.002

Li M, Wang Y, Liu Y, Wang H, Song H (2022) Preparation of active carbon through one-step NaOH activation of coconut shell biomass for phenolic wastewater treatment. Res Chem Intermed 48(4):1665–1684. https://doi.org/10.1007/s11164-021-04650-0

Lin HC, Hu JS, Lee WJ, Peng CW, Lai YJ, Wu SC, Fujimoto N (2015) Adsorption characteristics and pore structure of activated carbons prepared from sorghum distillery residue. J Fac Agric Kyushu Univ 60(1):173–182. https://doi.org/10.5109/1526300

Liu B, Younis SA, Lee J, Szulejko JE, Dou X, Kim KH (2021) The competing role of moisture in adsorption of gaseous benzene on microporous carbon. Sep Purif Technol 277:119487. https://doi.org/10.1016/j.seppur.2021.119487

Lobato-Peralta DR, Duque-Brito E, Villafan-Vidales HI, Longoria A, Sebastian PJ, Cuentas-Gallegos AK, Arancibia-Bulnes CA, Okoye PU (2021) A review on trends in lignin extraction and valorization of lignocellulosic biomass for energy applications. J Clean Prod 293:126123. https://doi.org/10.1016/j.jclepro.2021.126123

Long L, Xue Y, Hu X, Zhu Y (2019) Study on the influence of surface potential on the nitrate adsorption capacity of metal modified biochar. Environ Sci Pollut Res 26:3065–3074

Lucialli P, Marinello S, Pollini E, Scaringi M, Sajani SZ, Marchesi S, Cori L (2020) Indoor and outdoor concentrations of benzene, toluene, ethylbenzene and xylene in some Italian schools evaluation of areas with different air pollution. Atmos Pollut Res 11(11):1998–2010. https://doi.org/10.1016/j.apr.2020.08.007

Lv Y, Sun J, Yu G, Wang W, Song Z, Zhao X, Mao Y (2020) Hydrophobic design of adsorbent for VOC removal in humid environment and quick regeneration by microwave. Microporous Mesoporous Mater 294:109869. https://doi.org/10.1016/j.micromeso.2019.109869

Maia LS, Duizit LD, Pinhatio FR, Mulinari DR (2021) Valuation of banana peel waste for producing activated carbon via NaOH and pyrolysis for methylene blue removal. Carb Lett 31(4):749–762. https://doi.org/10.1007/s42823-021-00226-5

Maneerung T, Liew J, Dai Y, Kawi S, Chong C, Wang CH (2016) Activated carbon derived from carbon residue from biomass gasification and its application for dye adsorption: kinetics, isotherms and thermodynamic studies. Bioresour Technol 200:350–359. https://doi.org/10.1016/j.biortech.2015.10.047

Mishra RK, Mohanty K (2021) Fuel properties and compositional analysis of Areca catechu sawdust over MgO and ZSM-5 catalysts. J Energy Inst 94:252–262. https://doi.org/10.1016/j.joei.2020.09.009

Mishra RK, Mohanty K (2022) Pyrolysis of *Cascabela thevetia* seeds over ZSM-5 catalysts: fuel properties and compositional analysis. Biomass Convers Biorefinery 12(5):1449–1464. https://doi.org/10.1007/s13399-020-00841-8

Missia DA, Demetriou E, Michael N, Tolis EI, Bartzis JG (2010) Indoor exposure from building materials: a field study. Atmos Environ 44(35):4388–4395. https://doi.org/10.1016/j.atmosenv.2010.07.049

Muniandy L, Adam F, Mohamed AR, Ng EP (2014) The synthesis and characterization of high purity mixed microporous/mesoporous activated carbon from rice husk using chemical activation with NaOH and KOH. Microporous Mesoporous Mater 197:316–323. https://doi.org/10.1016/j.micromeso.2014.06.020

Nourmoradi H, Nikaeen M, Khiadani M (2012) Removal of benzene, toluene, ethylbenzene and xylene (BTEX) from aqueous solutions by montmorillonite modified with nonionic surfactant: equilibrium, kinetic and thermodynamic study. Chem Eng J 191:341–348. https://doi.org/10.1016/j.cej.2012.03.029

Pallarés J, González-Cencerrado A, Arauzo I (2018) Production and characterization of activated carbon from barley straw by physical activation with carbon dioxide and steam. Biomass Bioenerg 115:64–73. https://doi.org/10.1016/j.biombioe.2018.04.015

Park MH, Jeong S, Kim JY (2019) Adsorption of NH3-N onto rice straw-derived biochar. J Environ Chem Eng 7(2):103039. https://doi.org/10.1016/j.jece.2019.103039

Pathak PD, Mandavgane SA (2015) Preparation and characterization of raw and carbon from banana peel by microwave activation: application in citric acid adsorption. J Environ Chem Eng 3:2435–2447. https://doi.org/10.1016/j.jece.2015.08.023

Perkins AN, Inayat-Hussain SH, Deziel NC, Johnson CH, Ferguson SS, Garcia-Milian R, Thompson DC, Vasiliou V (2019) Evaluation of potential carcinogenicity of organic chemicals in synthetic turf crumb rubber. Environ Res 169:163–172. https://doi.org/10.1016/j.envres.2018.10.018

Pongener C, Bhomick PC, Supong A, Baruah M, Sinha UB, Sinha D (2018) Adsorption of fluoride onto activated carbon synthesized from *Manihot esculenta* biomass—equilibrium, kinetic and thermodynamic studies. J Environ Chem Eng 6(2):2382–2389. https://doi.org/10.1016/j.jece.2018.02.045

Potbhare AK, Chaudhary RG, Chouke PB, Yerpude S, Mondal A, Sonkusare VN, Ar R, Juneja HD (2019) Phytosynthesis of nearly monodisperse CuO nanospheres using Phyllanthus reticulatus/Conyza and its antioxidant/antibacterial assays. Mater Sci Eng C 99:783–793. https://doi.org/10.1016/j.msec.2019.02.010

Pui WK, Yusoff R, Aroua MK (2019) A review on activated carbon adsorption for volatile organic compounds (VOCs). Rev Chem Eng 35(5):649–668. https://doi.org/10.1515/revce-2017-0057

Qiang Z, Gurkan B, Ma J, Liu X, Guo Y, Cakmak M, Cavicchi KA, Vogt BD (2016) Roll-to-roll fabrication of high surface area mesoporous carbon with process-tunable pore texture for optimization of adsorption capacity of bulky organic dyes. Microporous Mesoporous Mater 227:57–64. https://doi.org/10.1016/j.micromeso.2016.02.015

Quan C, Su R, Gao N (2020) Preparation of activated biomass carbon from pine sawdust for supercapacitor and CO2 capture. Int J Energy Res 44(6):4335–4351. https://doi.org/10.1002/er.5206

Querejeta N, Gil MV, Pevida C, Centeno TA (2018) Standing out the key role of ultramicroporosity to tailor biomass-derived carbons for CO_2 capture. J CO2 Utilization 26:1–7. https://doi.org/10.1016/j.jcou.2018.04.016

Rajabi H, Mosleh MH, Prakoso T, Ghaemi N, Mandal P, Lea-Langton A, Sedighi M (2021) Competitive adsorption of multi-component volatile organic compounds on biochar. Chemosphere 283:131288. https://doi.org/10.1016/j.chemosphere.2021.131288

Rois MF, Widiyastuti W, Setyawan H, Rahmatika AM, Ogi T (2021) Preparation of activated carbon from alkali lignin using novel one-step process for high electrochemical performance application. Arab J Chem 14(6):103162. https://doi.org/10.1016/j.arabjc.2021.103162

Rovani S, Rodrigues AG, Medeiros LF, Cataluña R, Lima ÉC, Fernandes AN (2016) Synthesis and characterisation of activated carbon from agroindustrial waste—preliminary study of 17β-estradiol removal from aqueous solution. J Environ Chem Eng 4:2128–2137. https://doi.org/10.1016/j.jece.2016.03.030

Roy K, Verma KM, Vikrant K, Goswami M, Sonwani RK, Rai BN, Vellingiri K, Kim KH, Giri BS, Singh RS (2018) Removal of patent blue (V) dye using Indian bael shell biochar: characterization, application and kinetic studies. Sustainability 10(8):2669. https://doi.org/10.3390/su10082669

Ruiz-Jimenez J, Heiskanen I, Tanskanen V, Hartonen K, Riekkola ML (2022) Analysis of indoor air emissions: from building materials to biogenic and anthropogenic activities. J Chromatogr Open 2:100041. https://doi.org/10.1016/j.jcoa.2022.100041

Sadezky A, Muckenhuber H, Grothe H, Niessner R, Pöschl U (2005) Raman microspectroscopy of soot and related carbonaceous materials: spectral analysis and structural information. Carbon 43(8):1731–1742. https://doi.org/10.1016/j.carbon.2005.02.018

Saha D, Mirando N, Levchenko A (2018) Liquid and vapor phase adsorption of BTX in lignin derived activated carbon: equilibrium and kinetics study. J Clean Prod 182:372–378. https://doi.org/10.1016/j.jclepro.2018.02.076

Saleh TA (2018) Simultaneous adsorptive desulfurization of diesel fuel over bimetallic nanoparticles loaded on activated carbon. J Clean Prod 172:2123–2132. https://doi.org/10.1016/j.jclepro.2017.11.208

Schifter I, Díaz L, Rodríguez R, González-Macías C (2014) The contribution of evaporative emissions from gasoline vehicles to the volatile organic compound inventory in Mexico City. Environ Monit Assess 186:3969–3983. https://doi.org/10.1007/s10661-014-3672-2

Senthilkumar ST, Senthilkumar B, Balaji S, Sanjeeviraja C, Selvan RK (2011) Preparation of activated carbon from sorghum pith and its structural and electrochemical properties. Mater Res Bull 46(3):413–419. https://doi.org/10.1016/j.materresbull.2010.12.002

Serafin J, Narkiewicz U, Morawski AW, Wróbel RJ, Michalkiewicz B (2017) Highly microporous activated carbons from biomass for CO_2 capture and effective micropores at different conditions. J CO2 Utilization 18:73–79. https://doi.org/10.1016/j.jcou.2017.01.006

Serafin J, Baca M, Biegun M, Mijowska E, Kaleńczuk RJ, Sreńscek-Nazzal J, Michalkiewicz B (2019) Direct conversion of biomass to nanoporous activated biocarbons for high CO_2 adsorption and supercapacitor applications. Appl Surf Sci 497:143722. https://doi.org/10.1016/j.apsusc.2019.143722

Shoaib AG, El-Sikaily A, El Nemr A, Mohamed AEDA, Hassan AA (2020) Preparation and characterization of highly surface area activated carbons followed type IV from marine red alga (*Pterocladia capillacea*) by zinc chloride activation. Biomass Convers Biorefinery 12:2253–2265. https://doi.org/10.1007/s13399-020-00760-8

Sonkusare VN, Chaudhary RG, Bhusari GS, Mondal A, Potbhare AK, Mishra RK, Juneja HD, Abdala AA (2020) Mesoporous octahedron-shaped tricobalt tetroxide nanoparticles for photocatalytic degradation of toxic dyes. ACS Omega 5(14):7823–7835. https://doi.org/10.1021/acsomega.9b03998

Sophia C, Lima EC (2018) Removal of emerging contaminants from the environment by adsorption. Ecotoxicol Environ Saf 150:1–17. https://doi.org/10.1016/j.ecoenv.2017.12.026

Sun Y, Su G, He Z, Wei Y, Hu J, Liu H, Liu G (2022) Porous carbons derived from desiliconized rice husk char and their applications as an adsorbent in multivalent ions recycling for spent battery. J Chem. https://doi.org/10.1155/2022/822508854

Takaya CA, Fletcher LA, Singh S, Okwuosa UC, Ross AB (2016) Recovery of phosphate with chemically modified biochars. J Environ Chem Eng 4(1):1156–1165. https://doi.org/10.1016/j.jece.2016.01.011

Tang Z, Gao J, Zhang Y, Du Q, Feng D, Dong H, Peng Y, Zhang T, Xie M (2023) Ultra-microporous biocharbased carbon adsorbents by a facile chemical activation strategy for high-performance CO_2 adsorption. Fuel Process Technol 241:107613. https://doi.org/10.1016/j.fuproc.2022.107613

Tsoncheva T, Mileva A, Tsyntsarski B, Paneva D, Spassova I, Kovacheva D, Velinov N, Karashanova D, Georgieva B, Petrov N (2018) Activated carbon from Bulgarian peach stones as a support of catalysts for methanol decomposition. Biomass Bioenerg 109:135–146. https://doi.org/10.1016/j.biombioe.2017.12.022

Ukanwa KS, Patchigolla K, Sakrabani R, Anthony E, Mandavgane S (2019) A review of chemicals to produce activated carbon from

agricultural waste biomass. Sustainability 11(22):6204. https://doi.org/10.3390/su11226204

USEPA (1999) Compendium method TO-17 determination of volatile organic compounds in ambient air using active sampling onto sorbent tubes. US Environmental Protection Agency technical assistance document. EPA/625/R-96/010b

Ushiki I, Ota M, Sato Y, Inomata H (2014) A kinetic study of organic compounds (acetone, toluene, *n*-hexane and *n*-decane) adsorption behavior on activated carbon under supercritical carbon dioxide conditions at temperature from 313 to 353 K and at pressure from 4.2 to 15.0 MPa. J Supercrit Fluids 95:187–194. https://doi.org/10.1016/j.supflu.2014.08.021

Valencia A, Muñiz-Valencia R, Ceballos-Magaña SG, Rojas-Mayorga CK, Bonilla-Petriciolet A, González J, Aguayo-Villarreal IA (2022) Cyclohexane and benzene separation by fixed-bed adsorption on activated carbons prepared from coconut shell. Environ Technol Innov 25:102076. https://doi.org/10.1016/j.eti.2021.102076

Vikrant K, Kim KH, Ok YS, Tsang DC, Tsang YF, Giri BS, Singh RS (2018) Engineered/designer biochar for the removal of phosphate in water and wastewater. Sci Total Environ 616:1242–1260. https://doi.org/10.1016/j.scitotenv.2017.10.193

Vilella PC, Lira JA, Azevedo DC, Bastos-Neto M, Stefanutti R (2017) Preparation of biomass-based activated carbons and their evaluation for biogas upgrading purposes. Ind Crops Prod 109:134–140. https://doi.org/10.1016/j.indcrop.2017.08.017

Wan Ibrahim WMH, Mohamad Amini MH, Sulaiman NS, Kadir WRA (2019) Powdered activated carbon prepared from *Leucaena leucocephala* biomass for cadmium removal in water purification process. Arab J Basic Appl Sci 26(1):30–40. https://doi.org/10.1080/25765299.2018.1533203

Wei X, Huang S, Yang J, Liu P, Li X, Xue R, Wang Y, Chen L, Chen X, Wu Y, Wu S (2023) Adsorption of methylene blue on activated carbons prepared from penicillin mycelial residues via torrefaction and hydrothermal pretreatment. Biomass Convers Biorefinery. https://doi.org/10.1007/s13399-023-03998-0

Wickliffe JK, Stock TH, Howard JL, Frahm E, Simon-Friedt BR, Montgomery K, Wilson MJ, Lichtveld MY, Harville E (2020) Increased long-term health risks attributable to select volatile organic compounds in residential indoor air in southeast Louisiana. Sci Rep 10(1):21649. https://doi.org/10.1038/s41598-020-78756-7

Wongcharee S, Aravinthan V, Erdei L, Sanongraj W (2018) Mesoporous activated carbon prepared from macadamia nut shell waste by carbon dioxide activation: comparative characterisation and study of methylene blue removal from aqueous solution. Asia-Pac J Chem Eng 13(2):e2179. https://doi.org/10.1002/apj.2179

Wu M, Zhao Z, Cai G, Wang C, Cheng G, Wang X (2022) Adsorption behaviour and mechanism of benzene, toluene and m-xylene (BTX) solution onto kaolinite: experimental and molecular dynamics simulation studies. Sep Purif Technol 291:120940. https://doi.org/10.1016/j.seppur.2022.120940

Xie H, Li N, Chen X, Jiang J, Zhao X (2020) Surface oxygen vacancies promoted photodegradation of benzene on TiO_2 film. Appl Surf Sci 511:145597. https://doi.org/10.1016/j.apsusc.2020.145597

Xu B, Chen Y, Wei G, Cao G, Zhang H, Yang Y (2010) Activated carbon with high capacitance prepared by NaOH activation for supercapacitors. Mater Chem Phys 124(1):504–509. https://doi.org/10.1016/j.matchemphys.2010.07.002

Yue T, Yue X, Chai F, Hu J, Lai Y, He L, Zhu R (2017) Characteristics of volatile organic compounds (VOCs) from the evaporative emissions of modern passenger cars. Atmos Environ 151:62–69. https://doi.org/10.1016/j.atmosenv.2016.12.008

Zhang R, Zeng L, Wang F, Li X, Li Z (2022) Influence of pore volume and surface area on benzene adsorption capacity of activated carbons in indoor environments. Build Environ 216:109011. https://doi.org/10.1016/j.buildenv.2022.109011

Zhang X, Rao R, Gao B, Ma S, Bi F, Li C, Zhu Z, Liu N, Yang Y, Wang Z (2023) Crystal engineering of TiO_2 enhanced photothermal catalytic degradation of DEHP on Pt catalysts. Mater Today Chem 34:101755. https://doi.org/10.1016/j.mtchem.2023.101755

Zhang X, Gao B, Rao R, Bi F, Li C, Yue K, Wang Y, Xu J, Feng X, Yang Y (2024) Defects materials of Institut Lavoisier-125 (Ti) materials enhanced photocatalytic activity for toluene and chlorobenzene mixtures degradation: mechanism study. J Colloid Interface Sci 660:423–439. https://doi.org/10.1016/j.jcis.2024.01.012

Zheng W, Li XM, Wang F, Yang Q, Deng P, Zeng GM (2008) Adsorption removal of cadmium and copper from aqueous solution by areca—a food waste. J Hazard Mater 157(2–3):490–495. https://doi.org/10.1016/j.jhazmat.2008.01.029